Lattice dynamics and Born instability in yttrium aluminum garnet, $Y_3A1_5O_{12}$

2010 J. Phys.: Condens. Matter 22 065401

(http://iopscience.iop.org/0953-8984/22/6/065401)

IOP PUBLISHING JOURNAL OF PHYSICS: CONDENSED MATTER

J. Phys.: Condens. Matter **22** (2010) 065401 (11pp) doi:10.1088/0953-8984/22/6/065401

Lattice dynamics and Born instability in yttrium aluminum garnet, $Y_3Al_5O_{12}$

Prabhatasree Goel, R Mittal, N Choudhury and S L Chaplot

Solid State Physics Division, Bhabha Atomic Research Centre, Trombay, Mumbai 400085, India

Received 6 October 2009, in final form 30 November 2009
Published 21 January 2010
Online at stacks.iop.org/JPhysCM/22/065401

Abstract

We report lattice dynamics calculations of various microscopic and macroscopic vibrational and thermodynamic properties of yttrium aluminum garnet (YAG), $Y_3Al_5O_{12}$, as a function of pressure up to 100 GPa and temperature up to 1500 K. YAG is an important solid-state laser material with several technological applications. Garnet has a complex structure with several interconnected dodecahedra, octahedra and tetrahedra. Unlike other aluminosilicate garnets, there are no distinct features to distinguish between intramolecular and intermolecular vibrations of the crystal. At ambient pressure, low energy phonons involving mainly the vibrations of yttrium atoms play a primary role in the manifestations of elastic and thermodynamic behavior. The aluminum atoms in tetrahedral and octahedral coordination are found to be dynamically distinct. Garnet's stability can be discerned from the response of its phonon frequencies to increasing pressure. The dynamics of both octahedral and tetrahedral aluminum atoms undergo radical changes under compression which have an important bearing on their high pressure and temperature properties. At 100 GPa, YAG develops a large phonon bandgap (90–110 meV) and its microscopic and macroscopic physical properties are found to be profoundly different from that at the ambient pressure phase. There are significant changes in the high pressure thermal expansion and specific heat. The mode Grüneisen parameters show significant changes in the low energy range with pressure. Our studies show that the YAG structure becomes mechanically unstable around $P = 108$ GPa due to the violation of the Born stability criteria. Although this does not rule out thermodynamic crossover to a lower free energy phase at lower pressure, this places an upper bound of $P = 110$ GPa for the mechanical stability of YAG.

(Some figures in this article are in colour only in the electronic version)

1. Introduction

Yttrium aluminum garnet ($Y_3Al_5O_{12}$) is an important solid-state laser host [1, 2] material. Nd-doped YAG has widespread use in commercial, medical, military and industrial applications. A combination of the ideal spectroscopic properties of the rare-earth ions in the YAG crystal, low thermal expansion, high optical transparency, low acoustic loss, high threshold for optical damage, hardness, and stability against chemical and mechanical changes make it the most widely used laser material [3–10]. They are hard, stable, isotropic and their large thermal conductivities permit laser operation at high power levels. Being one of the most creep-resistant [9] oxides, it finds application in high temperature ceramic composites [11]. Various doped YAG materials have been proposed as optical pressure sensors up to very high pressures of the order of 180 GPa [12, 13]. Garnets find use as geobarometers [14, 15], forming a part of the mantle transition region in the pressure range between 10 and 25 GPa [16, 17].

Owing to its numerous practical applications, a thorough understanding of the vibrational properties and high temperature, high pressure behavior becomes vital. Several studies with the aim of understanding the influence of defects due to doping have already been reported [18–26]. A better understanding of the parent compound would allow insights into the changes occurring in the solid-state properties of the crystal on doping. This information would further help in improving the usefulness of the doped YAG systems that find varied technological applications. Various workers have reported experimental x-ray and neutron diffraction [27–29], Brillouin

scattering and ultrasonic studies [30, 31], Raman [32] and infrared spectroscopy [5, 30–33], and measurements of the specific heat [34] and thermal expansion [35] of YAG. Theoretical studies of the electronic structure of pure garnets [3, 8, 10] and symmetry based studies on the vibrational properties of several rare-earth garnets [36–41] have also been reported.

The behavior of garnets under pressure has always been a subject of interest. Many garnets like Fe-rich YIG [42], gallium garnet (GGG) [28], etc, are found to undergo pressure-induced amorphization. But experimental studies indicate that YAG-based materials are stable under fairly high pressures, as high as 180 GPa [12]. It is found to be thermally stable up to high temperatures [34, 35] as well. Pressure-induced amorphization has been studied in a number of model systems like α-quartz, ice, etc, and it has been observed that the onset of pressure-induced amorphization coincides with zone boundary phonon softening and elastic instabilities [43, 44].

A comprehensive lattice dynamics study of pristine YAG, aimed at understanding its vibrational spectra, elasticity and thermodynamical properties at high pressure and temperature, has been scarce. Our work reports an extensive study of the structure, vibrational and thermodynamic properties of YAG, in detail. We have calculated the pressure dependence of phonon frequencies in the whole Brillouin zone. Such extensive calculations of the phonon dispersion relation in the various symmetry directions, phonon density of states and thermodynamic properties of YAG has not been reported till now. All reported [45–56] *ab initio* works on various garnet structured materials, including YAG, have mainly been restricted to structural and electronic properties. There are only a few studies [49, 53–56] on phonons and, due to the complex structures involved, these workers report calculations of only the long wavelength phonons, i.e. at the zone center. There are no reported high pressure *ab initio* studies on the dynamics and elastic properties of YAG. This work is an effort to understand the basic phonon-related properties in pure YAG. Thus, this paper is an attempt to fill the lacuna.

Microscopic understanding of the thermodynamic, high pressure properties of these garnets is essential for the quantitative understanding of its variety of properties. Accurate characterization of the structural, vibrational and thermodynamic properties is essential for understanding the physics involving these garnets. Extending on our earlier studies on aluminosilicate [14, 15] garnets, we have carried out detailed lattice dynamical calculations using a transferable shell model. These studies are fairly involved as these garnets have complex crystal structures with a large number of atoms in the primitive cell. We have calculated the crystal structure, elastic constants and density of states. Thermodynamic properties including the equation of state, specific heat and thermal expansion have also been computed. Our aim in the study has been to model the ambient phase, extrapolate the model calculations to high pressure and temperature, search for dynamical instabilities and understand the changes occurring in the bonding with increasing pressure and temperature. We have also tried to understand the response of the various Raman-active frequencies to pressure. Details of the lattice dynamical model calculations have been given in section 2, followed by results and discussions in section 3. Section 4 draws the various conclusions inferred therein.

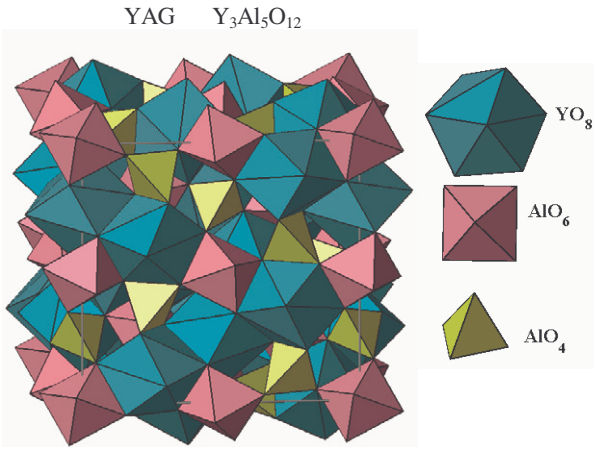

Figure 1. Polyhedral representations of the crystal structure of YAG.

2. Theoretical calculations

The general garnet crystal has a chemical formula $A_3B'_2B''_3O_{12}$, space group *Ia3d* [27], as shown in figure 1. The cubic cell contains eight formula units with the metal ions occupying different symmetry sites. The structure can be viewed as interconnected dodecahedra (at the A site), octahedra (at the B' site) and tetrahedra (at the B'' site) with shared O atoms at the corners of the polyhedra. Each oxygen atom is a member of two dodecahedra, one octahedron and one tetrahedron. There are three main classes of synthetic garnets based on the atomic species at the B'' sites. They are the aluminum garnets, iron garnet and gallium garnets. In the case of YAG, the B' and B'' sites are both occupied by the same element (aluminum) in different valence states. These have a complex structure with 80 atoms/primitive cell.

Lattice dynamics calculations of the equation of state and vibrational properties may be undertaken using either a quantum mechanical *ab initio* approach or an atomistic approach involving a semi-empirical interatomic potential. Owing to the structural complexity of garnets (80 atoms/primitive cell), we have used an atomistic approach. The interatomic potential consists of Coulombic and short-ranged Born–Mayer-type interactions along with a van der Waals interaction term (only between the oxygen atoms) [57, 58]. The parameters used in this study have been adjusted to satisfy the conditions of static and dynamical equilibrium. These calculations have been carried out using the current version of the software DISPR [59] developed at Trombay. The form of the interatomic potential is as follows:

$$V(r_{ij}) = \frac{e^2}{4\pi\varepsilon_0}\frac{Z(k)Z(k')}{r_{ij}} + a\exp\left[\frac{-br_{ij}}{R(k)+R(k')}\right] - \frac{C}{r_{ij}^6} \quad (1)$$

where r_{ij} is the separation between any two atoms, i and j, of type k and k', respectively. $R(k)$ and $Z(k)$ are the effective radius and charge of atoms of type k. The parameter

Table 1. Model parameters (Al(1) and Al(2) are in the octahedral and tetrahedral positions, respectively).

	Al(1)	Al(2)	O	Y
Z	1.7	2.556	−1.5475	2.5
R (Å)	1.3	1.05	1.89	2.0

$a = 1822$ eV and $b = 12.364$ have been treated as constants; this choice has been successfully used in earlier phonon studies of several complex solids [57, 58]. The effective charge and radius parameters used in the calculations are given in table 1. The van der Waals interaction terms have been introduced only between the oxygen atoms with $C = 100$ eV Å^6. The polarizability [60, 61] of the oxygen atoms has been introduced in the framework of the shell model with the shell charge $Y(\mathrm{O}) = -2.00$ and shell–core force constant $K(\mathrm{O}) = 110$ eV Å^{-2}.

The equilibrium crystal structure of YAG has been calculated by minimizing the Gibbs free energy at $T = 0$ K with respect to the lattice parameters and the atomic positions. Since the structural energy minimization was done at $T = 0$ K, the vibrational contribution was not included to derive the structure as a function of pressure. We expect a small contribution from the quantum mechanical zero-point vibrations that we have ignored. The good agreement between the calculated and experimental pressure variation of Raman modes up to 20 GPa and equation of state up to 100 GPa (as discussed later) indicates that our interatomic potential model for YAG is valid at high pressures.

The phonon density of states is calculated by integration over all phonon modes in the complete Brillouin zone. The contribution from individual atom species k can be obtained as a partial density of states, which is given as

$$g_k(\omega) = c \int \sum_j |\vec{\xi}(\vec{q}(j,k))|^2 \delta(\omega - \omega_j(\vec{q}))\, \mathrm{d}\vec{q} \qquad (2)$$

where $\xi(k, qj)$ is the polarization vector of the phonon $\omega_j(q)$.

One important measure of the effect of temperature and pressure on structural and thermal properties is the Grüneisen parameter, as it links the microscopic properties, namely change in frequencies with macroscopic observables, like the thermal expansion coefficient. The volume coefficient of thermal expansion is given as

$$\alpha_{\mathrm{v}}(T) = \frac{1}{BV} \sum_i \gamma_i C_{\mathrm{v}_i}(T); \qquad i = qj \qquad (3)$$

where B is the bulk modulus, V is the atomic volume and C_{v_i} is the specific heat contribution from mode i. $\boldsymbol{\gamma}_i$ is the Grüneisen parameter for the j th phonon mode at wavevector $\mathbf{q}$ and is given by

$$\gamma_i = -\frac{\partial \ln \omega_i}{\partial \ln V}. \qquad (4)$$

The volume thermal expansion is determined by integrating over the contribution of phonons of wavevectors on a $4 \times 4 \times 4$ mesh in an octant of the cubic Brillouin zone. The phonon dispersion relation along various symmetry directions and the pressure dependence of the phonon frequencies has also been computed.

Table 2. Comparison of calculated (ambient as well as high pressure) structural parameters and average bond lengths with reported experimental and *ab initio* data under ambient conditions. For the space group *Ia3d*, the Y, Al(1), Al(2) and O atoms are located at Wyckoff positions 24(c) (0, 0.25, 0.125), 24(d) (0, 0, 0), 16(a) (0.375, 0, 0.25) and 96(h) (u, v, w), respectively.

P (GPa)	0 Experimental [27]	0 (*ab initio* [3, 8, 9])	0	50	110
Lattice parameter, a (Å)	12.0	11.904	11.96	11.24	10.78
u	0.9694		0.96	0.959	0.959
v	0.0512		0.047	0.054	0.056
w	0.15		0.16	0.159	0.157
Y–O (Å)	2.3675	2.37	2.36	2.24	2.15
Al(1)–O (Å)	1.9371	1.94	1.94	1.94	1.85
Al(2)–O (Å)	1.761	1.76	1.76	1.52	1.48

3. Results and discussions

3.1. Crystal structure and elastic constants

The computed garnet crystal structure is found to be in unison with experimental findings [27]. The calculated lattice constant and the fractional coordinates are found to be in good agreement with reported data, as can be seen from table 2. The elastic constants have been calculated from the slopes of the acoustic phonon branches and bulk modulus has been calculated analytically using the elastic constant values. The pressure derivative B' has been obtained numerically using the values of the bulk modulus at different pressures.

Numerical values of elastic constants for a cubic crystal are determined by the values of acoustic mode frequencies near the zone center along ⟨100⟩ and ⟨110⟩ crystallographic directions. Along ⟨100⟩ the longitudinal acoustic mode yields C_{11}, while the transverse mode gives C_{44}. The value $0.5(C_{11} - C_{12})$ is given by the transverse mode along ⟨110⟩ (with polarization along the ⟨$\bar{1}$10⟩ direction). The calculated elastic constants and bulk modulus are found to be comparable with reported values as shown in table 3a [30, 31, 3, 8]. C_{11} is the largest while C_{12} and C_{44} are comparable, as is generally found in most cubic crystals. The variation of elastic constants with pressure is plotted in figure 2. C_{11} and C_{12} vary linearly with pressure while C_{44} remains almost unchanged. The bulk modulus at 100 is 556 GPa, which is about three times its value at ambient pressure, so it becomes very hard compared to the ambient phase.

There are several definitions for elastic constants at high pressure. For cubic crystals the relevant elastic constants under hydrostatic pressure that define the Born stability criteria are $c_{11} = C_{11} - P$, $c_{12} = C_{12} + P$ and $c_{44} = C_{44} - P$, where C_{11}, C_{12} and C_{44} are the elastic constant values derived from the slopes of the acoustic phonon branches. For cubic crystals, under hydrostatic loading, the mechanical Born stability criteria [62] leads to $c_{11} + 2c_{12} > 0$, $c_{11} - c_{12} > 0$ and $c_{44} > 0$. For the system to be mechanically stable, all three of these conditions given above must be simultaneously satisfied. The Born stability criteria that are violated in the present case are that the parameter $c_{44} = C_{44} - P$ should

Table 3a. Comparison of elastic and Grüneisen parameter data. B and B' are the bulk modulus and its pressure derivative, respectively.

	Experimental	Calculated (this work)	Calculated (*ab initio* [3, 8])
C_{11} (GPa)	328[a], 339[b]	329	
C_{12} (GPa)	106[a], 114[b]	103	
C_{44} (GPa)	114[a], 116[b]	90	
B (GPa)	185[b], 189[c], 220[d]	178	220.7
B'	—	4.1	4.12
γ^{thermal}	1.43[a]	1.45	

[a] Reference [31]. [b] Reference [30]. [c] Reference [33]. [d] Reference [5].

be positive. This violation is found in the calculation at P above 108 GPa. Although C_{44} itself remains positive, the value of the pressure derivative of the elastic constant C_{44} is less than 1 as per our calculations; as a result the parameter $c_{44} = C_{44} - P$ is very close to zero at 100 GPa and becomes negative beyond 108 GPa. Figure 2 gives c_{11}, c_{12} and c_{44} for YAG under pressure; it can be see that c_{44} becomes negative around 108 GPa. Reported experimental [12] energy dispersive x-ray diffraction data suggests that long range crystalline order is lost beyond 100 GPa in Sm doped YAG.

The pressure derivatives of the computed elastic constants have been compared in table 3b (a) with those reported by Saunders *et al* [29] (calculated using a atomistic model) and with experimental (ultrasonic wave velocity measurements up to 0.15 GPa) results of Yogurtcu *et al* [31]. Our calculations are in good agreement with experimental values as well as with the previous calculations by Saunders *et al* (those obtained with 90% ionicity).

3.2. Long wavelength phonon frequencies

Corresponding to the 80 atoms in the garnet primitive cell, a total of 240 phonon modes occur at every wavevector. Group theoretical symmetry analysis was undertaken to classify the phonon modes belonging to various representations. Because of the selection rules only phonon modes belonging to certain group theoretical representations are active in typical single-crystal Raman, infrared and inelastic neutron scattering measurements. These selection rules are governed by the symmetry of the system and the scattering geometry employed. The theoretical scheme for the derivation of the symmetry vectors is based on irreducible multiplier representations [63–65] involving construction of symmetry

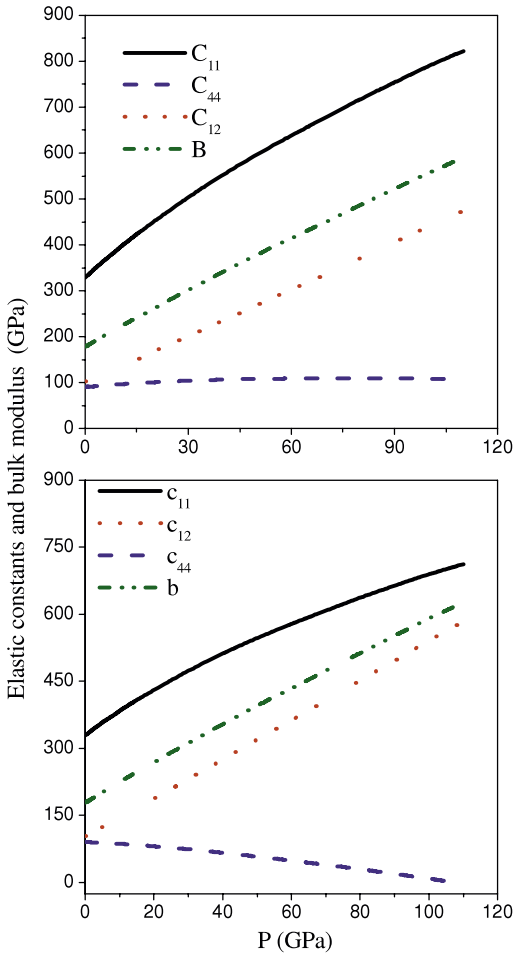

Figure 2. Pressure dependence of elastic constants and bulk modulus of YAG. For cubic crystals the relevant elastic constants under hydrostatic pressure that define the Born stability criteria are $c_{11} = C_{11} - P$, $c_{12} = C_{12} + P$ and $c_{44} = C_{44} - P$, $b = (c_{11} + 2c_{12})/3$, where C_{11}, C_{12} and C_{44} are the elastic constant values derived from the slopes of the acoustic phonon branches.

adapted vectors, which are used for block diagonalizing the dynamical matrix. This enables the assignment of the phonon modes belonging to various representations and direct comparison with observed single-crystal Raman and infrared data.

At the zone center, the phonon modes are classified into the following irreducible representations:

$$\Gamma : 3A_{1g} + 5A_{2g} + 5A_{2u} + 5A_{1u} + 8E_g + 14T_{2g} + 14T_{1g} + 10E_u + 18T_{1u} + 16T_{2u}.$$

Table 3b. Comparison of our calculations with those of Saunders *et al* [29] and with reported experiments [31]. γ^{el} is the average value of the Grüneisen constants of the acoustic modes.

	Lattice parameter (Å)	C_{11} (GPa)	C_{12} (GPa)	C_{44} (GPa)	B (GPa)	γ^{thermal}	γ^{el}	$\partial C_{11}/\partial P$	$\partial C_{12}/\partial P$	$\partial C_{44}/\partial P$	$\partial B/\partial P$
Saunders *et al* [a]	11.93	325	102.7	103	177	0.9	0.73	6.3	2.5	0.19	3.76
Saunders *et al* [b]	11.93	401	127	127	218	0.9	0.73	6.3	2.5	0.19	3.75
Yogurtcu *et al* [31]	12.0	328	106	114	180	1.43	0.727	6.31	3.51	0.62	4.42
This work	11.96	329	103	90	178	1.45	1.1	4.6	3.4	0.16	3.8

[a] 90% ionicity. [b] 100% ionicity.

Table 4. Comparison between experimental [41] and calculated Raman-active frequencies.

	$\omega_{i(\mathrm{exp})}$	$\omega_{i(\mathrm{cal})}$	$(\gamma_i)_{\mathrm{exp}}$	$(\gamma_i)_{\mathrm{cal}}$
T_{2g}	145	137	2.4	2.1
	220	214	1.6	2.0
	243	239	1.8	1.1
	261	254	1.1	1.4
	295	289	1.5	1.0
	372	353	1.6	0.8
	406	386	1.0	1.1
	—	477		0.4
	438	499	0.8	0.5
	545	594	0.8	0.6
	—	661		0.4
	691	705	1.4	0.8
	718	738	1.3	0.8
	857	886	1.0	0.5
E_{2g}	163	161	0.7	0.6
	310	261	1.6	1.3
	340	360	1.5	0.9
	402	386	1.1	1.0
	536	545	0.7	0.4
	—	633		0.3
	712	736	1.1	0.6
	754	803	1.3	0.7
A_{1g}	370	387	0.8	1.1
	559	569	0.8	0.5
	783	776	0.9	0.5

The $3A_{1g}$, $8E_g$ and $14T_{2g}$ are Raman-active while $18T_{1u}$ modes are infrared-active. The E modes are doubly degenerate while the T modes are triply degenerate. These modes have been experimentally [5, 32] measured and they compare (table 4) very well with our calculated values. However, there are no *ab initio* calculations of the long wavelength phonons for comparison. The calculated phonon frequencies with mode assignments are compared with the available Raman and infrared data [5, 32] in figure 3. Hurrell *et al* [32] have measured 15 of the IR modes using the near-normal reflection method. Hofmeister *et al* [5] have measured all the modes through a combination of reflection and absorption spectroscopy. The static ε_o, and high frequency ε_∞, dielectric constants are related to the infrared frequencies through the Lyddane–Sachs–Teller (LST) relation:

$$\prod_i \left(\frac{\nu_i(\mathrm{LO})}{\nu_i(\mathrm{TO})}\right)^2 = \frac{\varepsilon_o}{\varepsilon_\infty}. \tag{5}$$

The experimental value for YAG is 3.2 ([5] and references therein); the value calculated by Hurrell *et al* [32] using their measured frequencies is 3.96, while the one calculated by Hofmeister is 3.27. Our calculated value is 3.46. There appears to be no bandgaps in the frequency spectrum. Both the experimental studies as well as the calculations support this observation. This is against the general trend found in aluminosilicate garnets [14, 15], which show a bandgap in the 650–800 cm^{-1} frequency range. The low energy modes are in very good agreement with the experimental data. However, at the higher frequency region, the calculated values seem to be slightly different from experimental data. Our results are closer to Hofmeister [5] with a deviation of about 5%. As

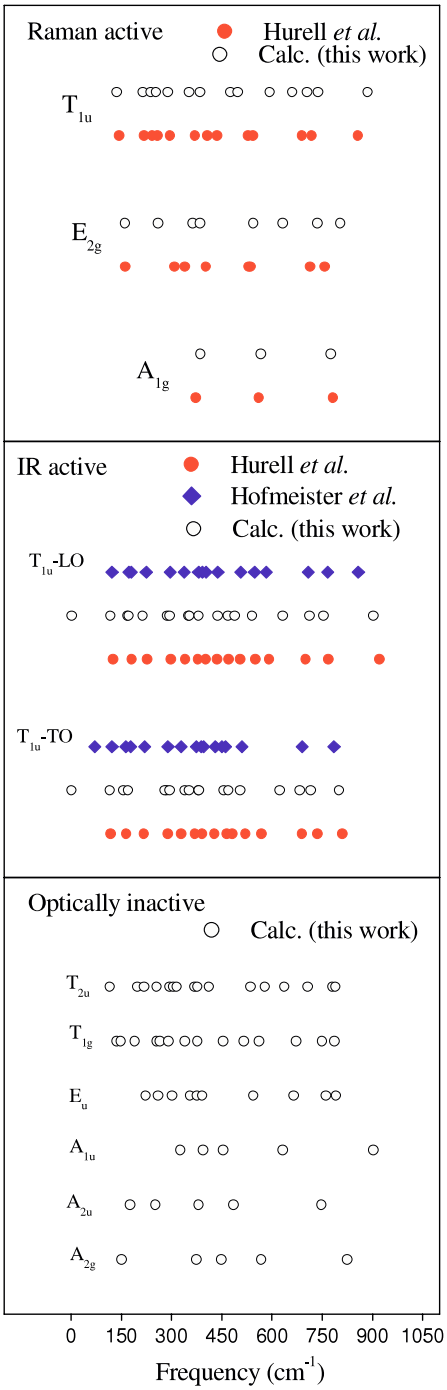

Figure 3. Phonon frequencies at the zone center compared with available experimental optical data [5, 32].

discussed above the Born instability criteria are related to the acoustic phonons at low frequencies only and so would not be affected. This would marginally affect the calculation of various thermodynamic properties (given below) like specific heat at high temperatures only.

The group theoretical classification in the three symmetry directions is as given below:

[010]: $29\Sigma_1 + 29\Sigma_2 + 29\Sigma_3 + 29\Sigma_4 + 62\Sigma_5$

(Σ_5 is doubly degenerate)

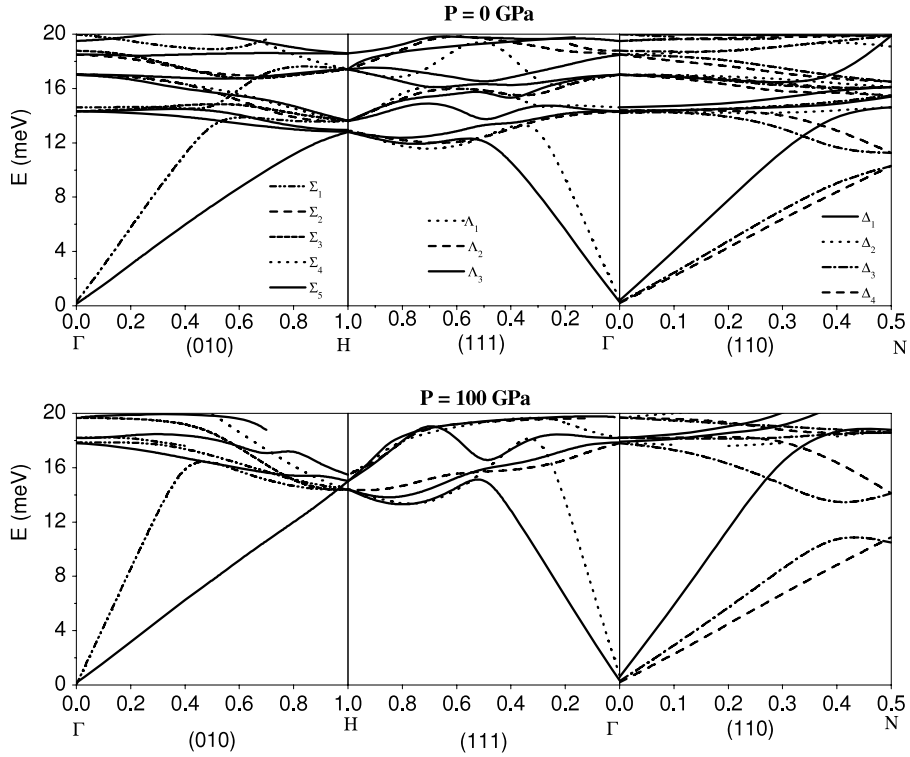

Figure 4. Phonon dispersion relation along the three high symmetry directions in the low energy range up to 20 meV at $P = 0$ and 100 GPa.

$$[111]: 40\Lambda_1 + 40\Lambda_2 + 80\Lambda_3\ (\Lambda_3 \text{ is doubly degenerate})$$

$$[110]: 59\Delta_1 + 59\Delta_2 + 61\Delta_3 + 61\Delta_4.$$

The calculated phonon dispersion relations in the high symmetry directions in the low energy range up to 20 meV, at $P = 0$ and 100 GPa, are shown in figure 4. It can be seen that many branches have hardened with pressure. There are no significant changes in any of the branches which might indicate a definite softening in any of the low energy branches. There is also no optical mode softening.

The calculated pressure dependence of phonon spectra, at ambient pressure, is used for calculation of the Grüneisen parameter $\Gamma(E)$, averaged for all phonons of energy E. The variation in the values of the Grüneisen values for all the modes is shown in figure 5. The energy of the modes can be divided into three groups: group I between 0 and 30 meV, group II corresponding to modes between 30 and 60 meV and group III for the modes >60 meV. The modes below 30 meV exhibit high values of Γ, with an average around 1.5; the average Γ of group II is around 1 and that of group III is 0.5.

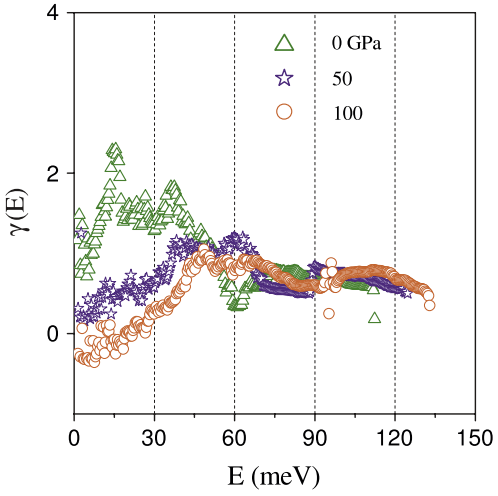

Figure 5. Variation in the calculated mode Grüneisen parameters at various pressures.

3.3. Phonon density of states, partial density of states and thermodynamic properties

The calculated total and partial phonon density of states are shown in figure 6. The solid line gives the density of states at ambient conditions. The dynamical contributions from the various species reveal separations in their spectral range. The yttrium atom contributes solely in the low energy region between 0 to 40 meV, with a minuscule contribution around 50 meV. Aluminum atoms with different coordinations contribute differently. Aluminum in the octahedral coordination contributes mainly between 30 and 70 meV, while the one in tetrahedral coordination contributes almost over the entire energy range, with a greater contribution on the higher energy end between 80 and 120 meV. Oxygen atoms contribute in the whole region from 0 to 120 meV. While the Al–O tetrahedral bond length is 1.76 Å, the Al–O octahedral bond length is 1.9 Å. These give rise to differences in their bonding characteristics and vibrational spectra. Modes

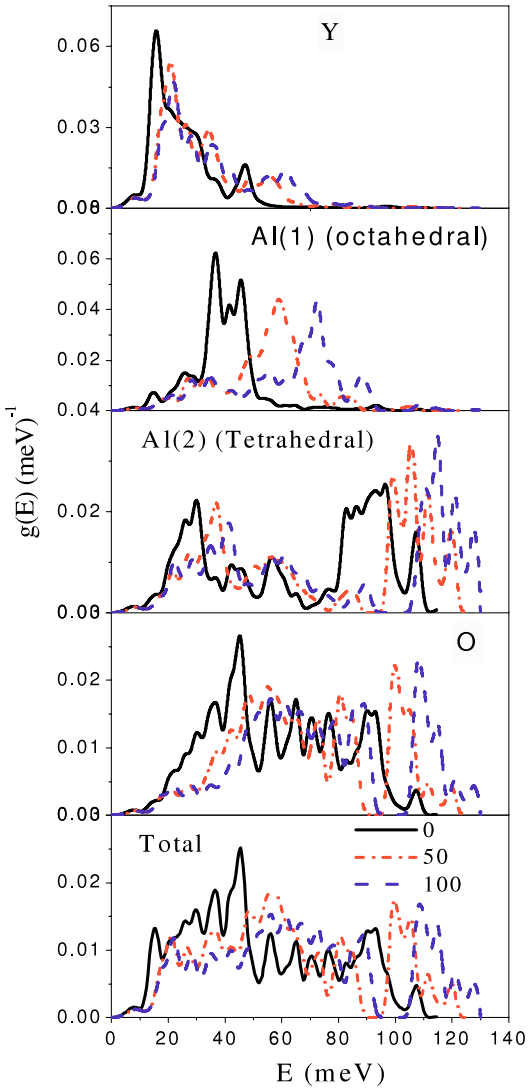

Figure 6. Total and partial phonon densities of state in YAG at $P = 0$, 50 and 100 GPa.

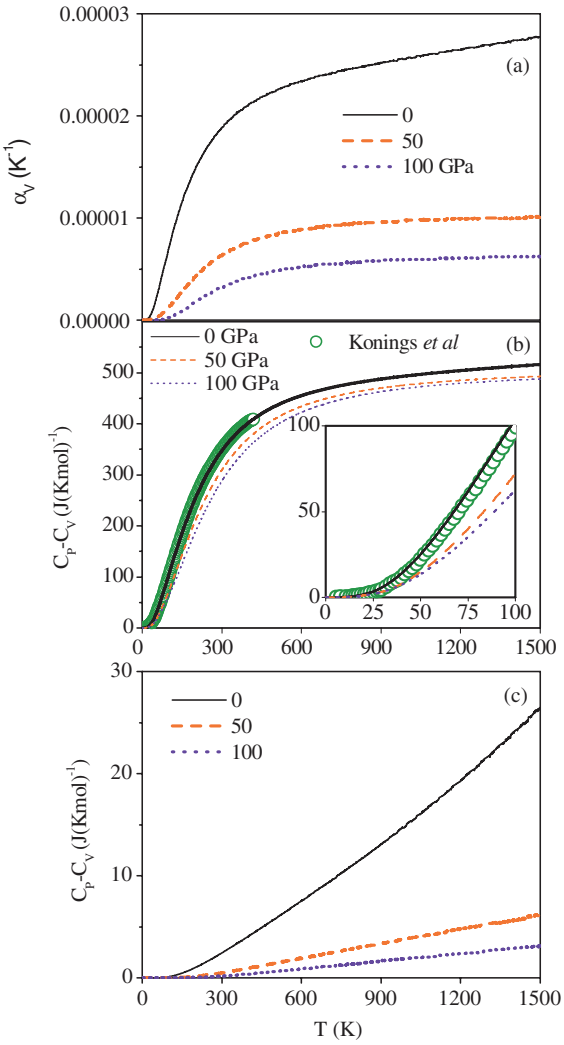

Figure 7. (a) Calculated volume thermal expansion coefficient (α_v) at different pressures. (b) Calculated specific heat at ambient condition in comparison with reported experimental (Konings *et al*) data [34]. Calculated specific heat at different high pressures has also been plotted for comparison. The inset gives the low temperature specific heat at various pressures. (c) Correction, C_P–C_V, due to implicit effects at various pressures.

in the intermediate region are due to a complex combination of vibrations involving all the polyhedra of Al and Y.

The computed one-phonon density of states, have been used for the calculation of the volume-dependent thermal expansion coefficient, specific heat and other thermodynamic properties. The calculated thermal expansion coefficient and specific heat has been shown in figures 7(a) and (b), respectively. The calculated specific heat is in excellent agreement with reported experimental data [34] as given in figure 7(b). The difference $C_p(T) - C_v(T)(=[\alpha_v(T)]^2 BVT)$ becomes significant at high temperatures and is about 5% in YAG.

Thermal expansion of a crystal arises from the anharmonicity of interatomic binding forces. A measure of anharmonicity [31] is given by a parameter called γ^{thermal} which is given as

$$\gamma^{\text{thermal}} = \beta V B^s / C_P \qquad (6)$$

where V is the atomic volume, B^s is the adiabatic bulk modulus, and β and C_P are the volume thermal expansion coefficient and specific heat at room temperature. Our calculations yield a value of 1.45 for γ^{thermal}, which is in excellent agreement with the reported [31] value of 1.43. The response of the crystal volume to temperature has been compared with experimental data [35] in figure 8. The calculations have been done in the quasiharmonic approximation using equation (3). The agreement is very good up to high temperatures of 1500 K (melting point for YAG is 2213 K). Thus, the percentage relative volume expansion is in excellent agreement with the reported experimental findings.

3.4. High pressure studies

The behavior of the 25 Raman modes ($3A_{1g} + 8E_g + 14T_{2g}$) under pressure have been studied and compared with reported data in figure 9. The majority of the experimental Grüneisen parameters vary between 0.6 and 1.7 while the calculated

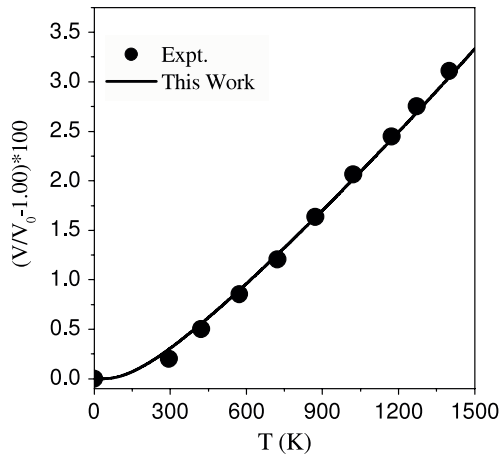

Figure 8. Thermal expansion of YAG in comparison with reported experimental (Geller *et al*) data [35].

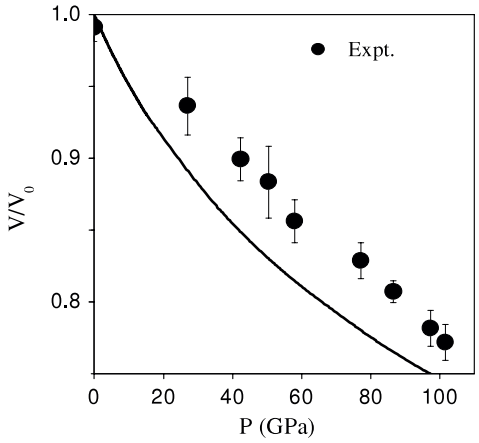

Figure 10. Calculated equation of state of YAG (full line) compared to reported experimental (Hua *et al*) data [28a] (solid circles).

values lie between 0.5 and 1.7. Only the lowest T_{2g} mode at 145 cm^{-1} has an experimental Grüneisen value of 2.4 whose corresponding calculated value is 2.1. The narrow range of these values show that the vibrational anharmonicity is similar for most of the optical phonons in this system.

Structural response of the garnet to an increase in pressure has been derived as in figure 10. YAG is reported to be a stable system [28] and is supposed to retain its cubic phase even beyond 100 GPa [28, 12]. The equation of state in YAG has been compared in figure 9 with reported [28a] data from synchrotron XRD experiments on Nd-doped YAG. Doping in rare-earth garnets is generally of the order of 1%. Elastic constants are observed to have negligible dependence on such small doping levels [28b]. Hence C_{44} of doped YAG [27] would be very close to that of pure YAG. The values of B_o and B' obtained from reported data using the Birch–Murughan equation are 383 and 1.77 GPa. These values are very different from the ones obtained by other experimentally reported data and our calculations. The experimental [28] equation of state suggests that a compression of ∼23% is obtained at 100 GPa, while at the same pressure the compression is 25%, as per our calculations.

At ambient conditions, there is no bandgap in the phonon density of states of YAG as seen in figure 6. The density of states of various atoms at $P = 50$ and 100 GPa have been plotted in figure 6. With increasing pressure, the low frequency density of states of the Y atom is significantly reduced and the peaks are shifted to higher energies. There is a shift of about 15–20 meV at $P = 50$ GPa as compared with $P = 0$ GPa. The YO_8 polyhedra experiences maximum compression between 0 and 50 GPa; thereafter it seems that the polyhedra are not as much compressible. Therefore the Y-PDOS does not change much between 50 and 100 GPa. The

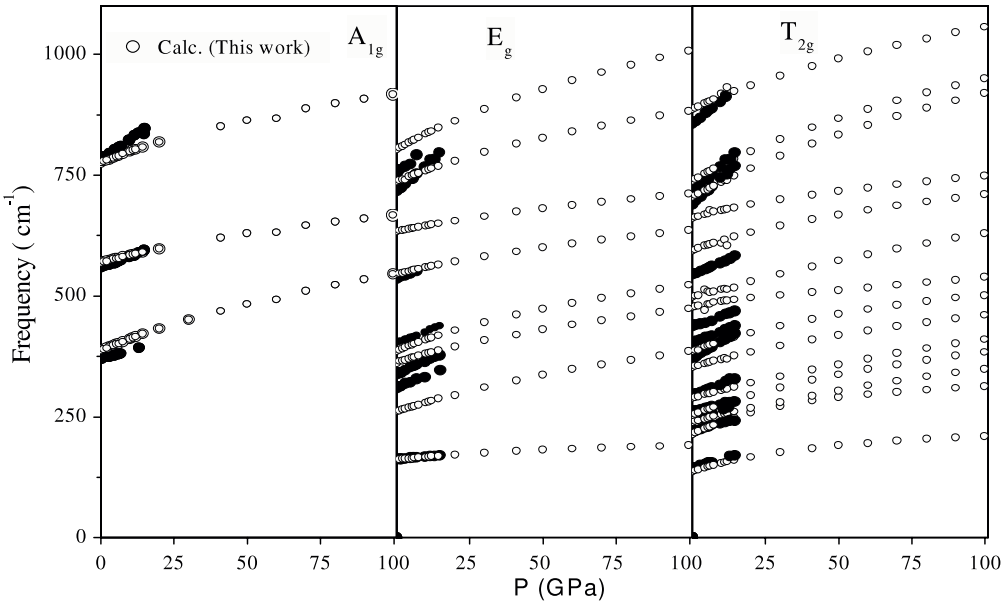

Figure 9. Pressure dependence of Raman modes in comparison with reported data. Open symbols are calculated values, while solid symbols [41] are reported experimental (Arvanitidis *et al*) values.

partial density of states of Al, in both octahedral and tetrahedral sites, is also significantly altered at high pressure and they seem to change continuously between 0 and 100 GPa. The O-PDOS also changes considerably with pressure, the peak around 40 meV reduces and the peak beyond 80 meV gains intensity with increasing pressure. The total density of states shows a bandgap between 90 and 100 meV at $P = 50$ GPa while the gap widens further up to 110 meV at 100 GPa.

The pressure dependence of mode Grüneisen parameters under different pressures has been plotted along with those at 0 GPa in figure 5. At 50 GPa, the average value between 0 and 30 meV is 0.5, between 30 and 60 meV it is 1 and beyond 60 most of the modes have a value around 0.5. At 100 GPa, the average value for modes between 0 and 30 meV is −0.25, between 30 and 60 meV, the average value is around 0, while for modes >60 meV the average value is around 0.75.

We can deduce that the maximum change seems to have occurred in the lowest-value energy modes below 30 meV, with some perceptible changes occurring in the highest energy modes. These modes mainly correspond to the YO_8 modes, and to the AlO_4 polyhedra. Thus this figure helps us to understand the microscopic scenario at these pressures. These changes in the vibrational spectra have an important bearing on its high pressure and high temperature properties. Our studies indicate significant atomic rearrangements in the AlO_6 and AlO_4 polyhedra, as well as the YO_8 dodecahedra. The opening of the phonon bandgap between 90 and 110 meV at 100 GPa is due to the Al(2)–O stretching vibrations shifting to higher energies.

Table 2 gives the structural parameters and the bond lengths at various pressures. The average bond lengths of the Y–O, Al(1)–O and Al(2)–O bonds have changed with increasing pressure. There are subtle readjustments and reorientations of the various polyhedral units.

The volume-dependent thermal expansion coefficient, specific heat and the correction, C_P–C_V, of YAG at high pressures have also been computed and compared with ambient phase values in figure 7. The ambient phase has the maximum thermal expansion coefficient. The correction, C_P–C_V (due to volume-dependent anharmonic effects), is maximum for the ambient phase and it decreases with increasing pressure. Thus, the specific heat decreases with increasing pressure. At lower temperatures below 100 K, the ambient phase has a higher specific heat, almost 1.5 times compared to that at 100 GPa. These results are consistent with the variations observed in the values of the mode Grüneisen constants.

In this work, we have provided an atomic level understanding of the macroscopic vibrational and thermodynamic properties of high pressure YAG, which have not been studied in detail earlier. Our studies indicate that the YAG structure is mechanically unstable at high pressures, due to violations of the Born stability criteria. Aluminosilicate garnets which are principal components of the Earth's mantle, are known to transform into an oxide phase along with chemical decomposition typically around 25–30 GPa [16]. Due to large kinetic hindrances, such a transformation has not been observed in YAG. Various previous works indicate that YAG may persist metastably up to high pressures of 180 GPa [12], while some of its diffraction peak [12] vanishes between 100 and 150 GPa [12]. The exact transition has not been observed experimentally so far, although high pressure diffraction experiments [12] indicate a disordered phase above $P = 100$ GPa.

Our theoretical calculations indicate that various polyhedral units contribute differently in different pressure regimes in YAG. There are significant changes in the phonon density of states with increasing pressure. Significant atomic rearrangements take place in the different polyhedral units as can be seen from their bond lengths and bond angles. While at ambient pressure the YO_8 dodecahedra strongly influence the elastic and thermodynamic properties, at higher pressures, the YO_8, AlO_6 and AlO_4 polyhedra continuously deform with pressure, giving rise to important manifestations in their elastic, vibrational and thermodynamic properties. We do not observe optical phonon softening up to fairly high pressures like 100 GPa. YAG, however, becomes mechanically unstable around 108 GPa (section 3.1) due to violation of the Born stability criteria. The c_{44} elastic constant involving a transverse acoustic phonon becomes soft under hydrostatic loading of 108 GPa and the structure becomes elastically unstable. This pressure is an upper bound for YAG retaining even a metastable garnet phase and a certain structural phase transition is indicated above this pressure although free energy crossover to a thermodynamically favorable phase at a lower pressure is not ruled out.

Under high pressures and temperatures, it is expected that cubic YAG would decompose into $3YAlO_3 + Al_2O_3$. Due to the large volume collapse of the perovskite structure, which is typically around 20% lower than the garnet volume, the PdV term would lower the free energy of the perovskite phase. The perovskite phase could thus remain the favored high pressure phase due to its dense atomic packing. However, due to the intrinsic complexity in dealing with chemical decomposition involved in this transition, theoretical studies of the exact pressure for such a garnet to perovskite crossover have not been undertaken for YAG.

High pressure YAG is significantly harder than the ambient phase (the bulk modulus at 100 GPa is three times its value at $P = 0$ GPa); the garnet to perovskite transition would involve a further substantial increase of the bulk modulus. The garnet GGG under dynamic compression has yielded a novel incompressible oxide phase with hardness greater than diamond [17]; perhaps similar phases with unusual hardness may be realized in YAG.

Our studies further indicate that the mechanical instability of YAG at high pressure is accompanied by large vibrational anharmonicity and changes in the mode Grüneisen parameters. The ambient phase mode Grüneisen values are all positive, while with increasing pressure many of the low energy modes (<30 meV) show negative values and some of the high energy modes (>60 meV) show a sharp increase. The middle range remains more or less unchanged. The calculated partial density of states (figure 6) shows that Y and Al(2) atoms mainly contribute below 30 meV and above 60 meV, respectively. The negative Γ values of low energy modes results in a lower value of overall positive thermal expansion coefficient, which in turn gives rise to a lower specific heat with increasing pressure.

4. Conclusions

We have reported detailed lattice dynamical calculations for the garnet YAG using a shell model. The calculated structure, elastic constants, phonon frequencies, specific heat, thermal expansion and equation of state of the ambient phase are in good agreement with available experimental data. At 100 GPa, YAG develops a large phonon bandgap (90–110 meV) and its microscopic and macroscopic physical properties are found to be profoundly different from that in the ambient pressure phase. Our detailed high pressure studies conclude that YAG is mechanically unstable beyond 108 GPa, due to the violation of the Born stability criteria. High pressure x-ray diffraction measurements [12] report the occurrence of a disordered phase between 100 and 150 GPa, and our studies suggest that these may perhaps be due to elastic instabilities.

Pressure-induced amorphization has been observed in GGG and YIG. However, the cubic garnet structure is found to be stable in YAG up to significantly higher pressures [28] and our studies reveal that up to 100 GPa there are no dynamical instabilities in YAG. Our results are in agreement with experimental studies [12] which have suggested that YAG undergoes a phase change to a disordered metastable phase between 100 and 150 GPa. The observed high pressure phase beyond 100 GPa has not been clearly understood [12]. The disordered phase perhaps occurs due to the large kinetic barriers for decomposition into the expected perovskite structure at high pressure.

Yttrium aluminum garnet (YAG) under ambient conditions shows differences with the previous calculations on aluminosilicate garnets [14, 15], namely there is no gap in the vibrational spectrum as seen in them. The Al atoms in tetrahedral and octahedral coordinations are dynamically distinct, with aluminum in the tetrahedral coordination contributing between 90 and 120 meV. Yttrium atoms contribute mainly in the low energy range, while intermediate energy states are due to a combination of movements of all the atoms. YAG is found to be thermally stable in the temperature range (up to 1500 K) studied. Grüneisen constants of the low energy modes (<30 meV) show great variation with increasing pressure, going from positive at 0 GPa to negative at 100 GPa. These modes become softer with pressure increase. The modes beyond 30 meV do not change much with changing pressure, excepting some modes which change drastically with increasing values of pressure. Thus, our results may have important implications for the proposed technological applications of YAG-based materials as pressure sensors over a wide range of pressures.

Although we have employed an atomistic approach, the model is in good agreement with experiments and reported *ab initio* [3, 8, 9] works (see tables 2, 3a and 3b). Furthermore the present work helps us to understand the dynamical characteristics associated with the high pressure disorder and pressure-induced amorphization. These aspects have not been clearly understood earlier. These results have important implications in the use of YAG as pressure sensors in the high pressure regime. The shell model successfully gives a fair and comprehensive description of the dynamics and various thermodynamic properties at high temperatures and pressures which are otherwise difficult to access experimentally. Our studies are able to interpret the complex high pressure data of YAG. This model may be used to study yttrium iron garnet (YIG) and other rare-earth garnets.

References

[1] Koechner W 2006 *Solid State Laser Engineering* (Berlin: Springer)
[2] Henderson B and Bartram R H 2000 *Crystal Field Engineering of Solid State Laser Materials* (Cambridge: Cambridge University Press)
[3] Xu Y-N and Ching W Y 1999 *Phys. Rev.* B **59** 10530
[4] Djemia P, Tetard F, Bouamama K, Charron E, Tetard D and Rabinovitch Y 2007 *J. Eur. Ceram. Soc.* **27** 4719
[5] Hofmeister A M and Campbell K R 1992 *J. Appl. Phys.* **72** 638
[6] McAloon B P and Hofmeister A M 1993 *Am. Mineral.* **78** 957
[7] Giesting P A and Hofmeister A M 2002 *Phys. Rev.* B **65** 144305
[8] Xu Y-N, Ching W Y and Brickeen B K 2000 *Phys. Rev.* B **61** 1817
[9] Dong J and Lu K 1991 *Phys. Rev.* B **43** 8808
[10] Ching W Y and Xu Y-N 1999 *Phys. Rev.* **59** 12815
[11] Parthasarthy T A, Mah T-I and Keller K 1992 *J. Am. Ceram. Soc.* **75** 1756
[12] Liu J and Vohra Y K 1994 *Appl. Phys. Lett.* **64** 3366
Liu J and Vohra Y K 1996 *J. Appl. Phys.* **79** 7978
Liu J and Vohra Y K 1996 *Solid. State Commun.* **88** 417
[13] Kobyakov S, Kaminska A, Suchocki A, Galanciak D and Malinowski M 2006 *Appl. Phys. Lett.* **88** 234102
[14] Mittal R, Chaplot S L, Choudhury N and Loong C K 2000 *Phys. Rev.* B **61** 3983
[15] Mittal R, Chaplot S L and Choudhury N 2001 *Phys. Rev.* B **64** 094302
[16] Irifune T, Higo Y, Inwe T, Kono Y, Ohfuji H and Funakoshi K 2008 *Nature* **451** 814
[17] Mashimo T, Chau R, Zang Y, Kobayoshi T, Sekine T, Fukuoka K, Syono Y, Kodama M and Nellis W J 2006 *Phys. Rev. Lett.* **96** 105504
[18] Chen J, Lu T C, Xu Y, Xu A G and Chen D A 2008 *J. Phys.: Condens. Matter* **20** 325212
[19] Wang C L, Solodovnikov D and Lynn K G 2005 *Phys. Rev.* B **73** 233204
[20] Anedda A, Carbonaro C M, Chiriu D, Corpino R, Marceddu M and Ricci R C 2006 *Phys. Rev.* B **74** 241508
[21] John Gruber B, Zandi B, Valiev U V and Rakhimov Sh A 2004 *Phys. Rev.* B **69** 115103
[22] Shen Y, Riedener T and Bray K L 2000 *Phys. Rev.* B **61** 11460
[23] Jun C, Dong-Quan C and Jing-Lin Z 2007 *Chin. Phys.* **16** 2779
[24] Schuh L, Metselaar R and Catlow C R A 1991 *J. Eur. Ceram. Soc.* **7** 67
[25] Kuklja M M 2000 *J. Phys.: Condens. Matter* **12** 2953
[26] Wang X-J, Dennis W M and Yen W M 1992 *J. Lumin.* **53** 44
[27] Euler F and Bruce J A 1965 *Acta Crystallogr.* **19** 971
[28a] Hua H, Mirov S and Vohra Y K 1996 *Phys. Rev.* B **54** 6200
[28b] Beghi M G, Bottani C E and Russo V 2000 *J. Appl. Phys.* **87** 1769
[29] Saunders G A, Parker S C, Benbattouche N and Alberts H I 1992 *Phys. Rev.* B **46** 8756
[30] Stoddart P R, Ngoepe P E, Mjwara P M, Comins J D and Saunders G A 1993 *J. Appl. Phys.* **73** 7298
[31] Yogurtcu Y K, Miller A J and Saunders G A 1980 *J. Phys. C: Solid State Phys.* **13** 6585

[32] Hurrell J P, Porto S P S, Chang I F, Mitra S S and Bauman R R 1968 *Phys. Rev.* **173** 851
[33] Alton W J 1967 *J. Appl. Phys.* **38** 3023
[34] Konings R J M, van der Laan R R, van Genderen A C G and van Miltenburg J C 1998 *Thermochim. Acta* **313** 201
[35] Geller S, Espinosa G P and Crandall P B 1969 *J. Appl. Crystallogr.* **2** 86
[36] Papagelis K 2002 *J. Phys.: Condens. Matter* **14** 915
Papagelis K 2002 *J. Phys.: Condens. Matter* **14** 3875
[37] Papagelis K 2003 *J. Phys. Chem. Solids* **64** 599
[38] Papagelis K and Ves S 2003 *J. Appl. Phys.* **94** 6491
[39] Papagelis K, Aravanitidis J, Kanellis G, Ves S and Kourouklis G A 2002 *J. Phys.: Condens. Matter* **14** 3875
[40] Papagelis K, Kanellis G, Arvanitidis J, Kourouklis G A and Ves S 1999 *Phys. Status Solidi* **215** 193
[41] Arvanitidis J, Papagelis K, Christofilos D, Kimura H, Kournouklis G A and Ves S 2004 *Phys. Status Solidi* b **241** 3149
[42] Gavriliuk A G, Struzhkin V V, Lyubutin I S and Trojan I A 2005 *JETP Lett.* **82** 603
[43] Chaplot S L and Sikka S K 1993 *Phys. Rev. Lett.* **71** 2674
[44] Choudhury N and Chaplot S L 2006 *Phys. Rev.* B **73** 094304
[45] Valenzano L, Meyer A, Demichelis R, Civalleri B and Dovesi R 2009 *Phys. Chem. Miner.* **36** 415
[46] Meyer A, Arco Ph D', Orlando R and Dovesi R 2009 *Theor. J. Phys. Chem.* C **113** 14507
[47] Chen J, Lu T C, Xu Y, Xu A G and Chen D Q 2008 *J. Phys.: Condens. Matter* **20** 325212
[48] Juhin A, Calas G, Cabaret D, Galoisy L and Hazemann J-L 2008 *Am. Miner.* **93** 800
[49] Zicovich-Wilson C M, Torres F J, Pascale F, Valenzano L, Orlando R and Dovesi R 2008 *J. Comput. Chem.* **9** 2268
[50] Dovesi R, Valenzano L, Pascale F, Ziovich-Wilson C M and Orlando R 2008 *J. Ram. Spec.* **40** 416
[51] Cristiglio V, Hennet L, Cuello G J, Johnson M R, Fernandez-Martinez A, Fischer H E, Pozdnyakova I, Zhanghi D, Brasaamin S, Brun J F and Price D L 2007 *J. Non. Cryst. Solids* **353** 1789
[52] Orlando R, Torres J, Pascale F, Ugliengo P, Ziovich-Wilson C M and Dovesi R 2006 *J. Phys. Chem.* B **110** 692
[53] Noel Y, Catti M, D'Arco Ph and Dovesi R 2006 *Phys. Chem. Miner.* **33** 383
[54] Vitos L, Magyari-Kope B, Ahuja R, Kollar J, Grimvall G and Johansson B 2006 *Phys. Earth Planet. Inter.* **156** 108
[55] Pascale F, Zicovich-Wilson C M, Orlando R, Roetti C, Ugliengo P and Dovesi R 2005 *J. Phys. Chem.* B **109** 6146
[56] Pascale F, Catti M, Damin A, Orlando R, Saunders V R and Dovesi R 2005 *J. Phys. Chem.* B **109** 18522
[57] Mittal R, Chaplot S L and Choudhury N 2006 *Prog. Mater. Sci.* **51** 211
[58] Chaplot S L, Choudhury N, Ghose S, Rao M N, Mittal R and Goel P 2002 *Eur. J. Mineral.* **14** 291
[59] Chaplot S L 1972 *Report BARC-972*
Chaplot S L 1992 unpublished
[60] Venkataraman G, Feldkamp L and Sahni V C 1975 *Dynamics of Perfect Crystals* (Cambridge: MIT Press)
[61] Bruesh P 1986 *Phonons: Theory and Experiments* (Berlin: Springer)
[62] Zhou Z and Joos B 1996 *Phys. Rev.* B **54** 3841
[63] Maradudin A A and Vosko S H 1968 *Rev. Mod. Phys.* **40** 1
[64] Kovalev O V 1964 *Irreducible Representations of Space Groups* (New York: Gordon and Breach)
[65] Bradley C J and Cracknell A P 1972 *The Mathematical Theory of Symmetry in Solids* (Oxford: Oxford University Press)